

Transition between Nonresonant and Resonant Charge Transport in Molecular Junctions

Songsong Li, Hao Yu, Jialing Li, Nicholas Angello, Edward R. Jira, Bo Li, Martin D. Burke, Jeffrey S. Moore, and Charles M. Schroeder*

Cite This: *Nano Lett.* 2021, 21, 8340–8347

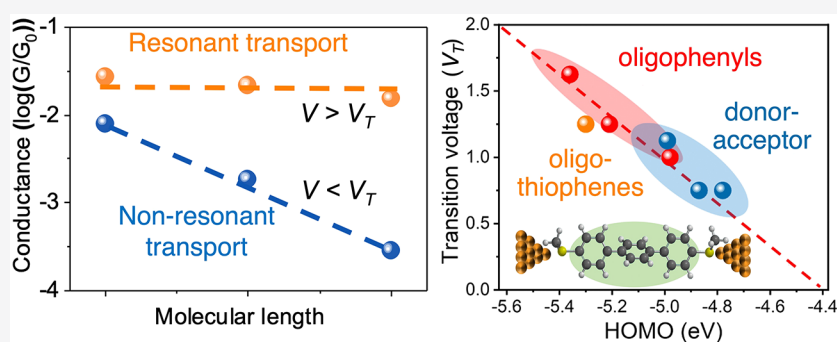
Read Online

ACCESS |

Metrics & More

Article Recommendations

Supporting Information



ABSTRACT: Efficient long-range charge transport is required for high-performance molecular electronic devices. Resonant transport is thought to occur in single molecule junctions when molecular frontier orbital energy levels align with electrode Fermi levels, thereby enabling efficient transport without molecular or environmental relaxation. Despite recent progress, we lack a systematic understanding of the transition between nonresonant and resonant transport for molecular junctions with different chemical compositions. In this work, we show that molecular junctions undergo a reversible transition from nonresonant tunneling to resonant transport as a function of applied bias. Transient bias-switching experiments show that the nonresonant to resonant transition is reversible with the applied bias. We determine a general quantitative relationship that describes the transition voltage as a function of the molecular frontier orbital energies and electrode Fermi levels. Overall, this work highlights the importance of frontier orbital energy alignment in achieving efficient charge transport in molecular devices.

KEYWORDS: molecular electronics, resonant transport, scanning tunneling microscope break-junction (STM-BJ)

Understanding intramolecular charge transport is essential for the design and development of new molecular electronic devices.^{1–4} Organic materials for molecular electronics are typically designed with highly delocalized conjugated backbones such as oligophenyls,^{5–7} oligothiophenes,⁸ oligoenes,^{9,10} polyporphyrins,^{11–14} and diketopyrrolopyrrole (DPP) oligomers.^{15,16} In general, conjugated organic molecules show a weaker length-dependent conductance decay compared to nonconjugated alkanes,¹⁷ which facilitates efficient long-range charge transport. In addition, low-resistance contacts such as Au–S,¹ Au–C,^{7,18,19} Ag–C,⁶ and Au–N²⁰ covalent linkages are used at molecule–electrode interfaces and exhibit 10–100 times lower contact resistance compared to contacts with Au–S¹ and Au–N^{5,17} dative linkages. Despite recent progress, the vast majority of prior work has focused on an understanding of nonresonant intramolecular charge transport or hopping transport mechanisms.²¹

Resonant transport holds the potential to enable highly efficient, long-range, and nearly length independent intra-

molecular charge transport. Resonant transport is realized when the energy of a frontier molecular orbital aligns with the electrode Fermi energy.^{22–24} Resonant transport has been reported in nanotubes,²⁵ DNA,²⁶ biphenyl-porphyrin oligomers (bp-ppo),²⁷ and donor–acceptor oligomers based on DPP,¹⁵ which remarkably show a nearly length-independent conductance over long distances beyond 10 nm. In theory, resonant transport can be achieved by tuning the applied bias across molecular junctions,^{20,27,28} thereby leading to alignment of molecular frontier orbital energies with the electrode Fermi levels. Recently, Zang et al.¹⁵ and Kuang et al.²⁷ reported the transition from nonresonant tunneling to resonant transport using high bias voltages in DPP and bp-ppo-based molecular

Received: July 28, 2021

Published: September 16, 2021



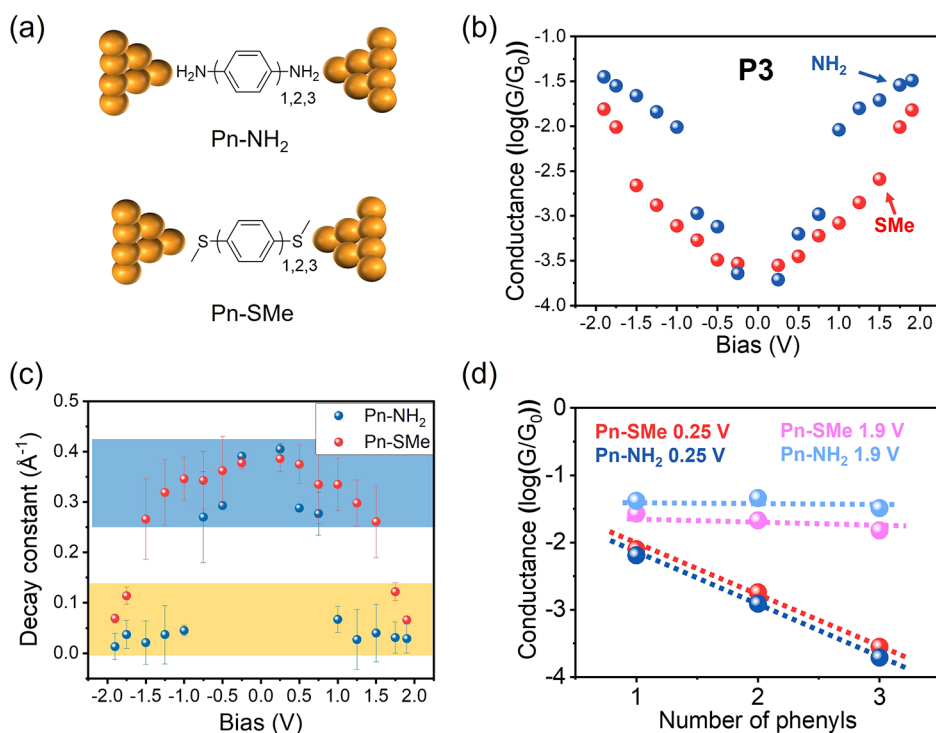


Figure 1. Single molecule charge transport experiments on amine- and thiomethyl-terminated oligophenyl junctions. (a) Schematic of amine and thiomethyl-terminated oligophenyls. (b) Conductance peak values for **P3** plotted as a function of applied bias from -1.9 V to $+1.9$ V on a semilog scale, with each data point constructed from >2000 traces. (c) Decay constant values of **Pn-NH₂** and **Pn-SMe** plotted as a function of applied bias from -1.9 V to $+1.9$ V on a semilog scale. The blue and yellow highlighted regions represent the length-dependent and nearly length-independent conductance behavior, respectively. (d) Conductance peak values of **Pn-NH₂** and **Pn-SMe** at 0.25 and 1.9 V bias are plotted as a function of the number of phenyls.

wires. Despite these observations, we lack a systematic understanding of the transition between nonresonant and resonant transport for junctions with different chemical compositions.

In this work, we study the nonresonant to resonant transition for a series of molecular junctions with different backbone compositions and frontier orbital energies. Interestingly, our results show that the transition voltage (V_T) follows a general linear relationship with the molecular frontier orbital energies. Our experimental results are consistent with a general physical model that considers the applied bias, electrode Fermi energies, and the strength and symmetry of the molecule-electrode coupling. Charge transport is characterized in molecular junctions based on para-linked oligophenyls and related control molecules terminated with amine (NH_2) and thiomethyl (SMe) anchors. At low applied bias, molecular conductance is length-dependent and decays exponentially as a function of molecular length. Upon increasing the applied bias in a stepwise fashion, remarkably high levels of conductance ($>10^{-2} G_0$) are observed, where G_0 is the quantum unit of conductance ($G_0 = 2e^2/h = 77.5 \mu\text{S}$). Interestingly, we observe a marked decrease in the length-dependent conductance decay constant (β) for amine- and thiomethyl-terminated *p*-terphenyl junctions at applied biases of 1 and 1.75 V, respectively, which suggests a transition from nonresonant to resonant transport. We further studied time-dependent, transient molecular conductance in bias-switching experiments using the holding mode of a scanning tunneling microscope-break junction (STM-BJ) instrument. Bias-switching experiments clearly show that the nonresonant to resonant transition is reversible as a function of applied bias. Taken together, our results show that

resonant transport offers an effective approach for achieving efficient long-range transport in molecular junctions.

A series of conjugated molecules was synthesized using reported methods or via iterative cross-coupling with MIDA boronates with automated catch-and-release purification²⁹ and characterized by ^1H and ^{13}C NMR spectroscopy (Supporting Information, Figures S1–S3). Following synthesis, we began by studying the charge transport properties of amine- (**Pn-NH₂**) and thiomethyl- (**Pn-SMe**) terminated oligophenyls ($n = 1, 2, 3$) attached to gold electrodes (Figure 1a) using a custom-built STM-BJ instrument, as previously described.^{16,30} In particular, we determined molecular conductance for **Pn-NH₂** and **Pn-SMe** oligophenyls (0.01 mM - 0.1 mM in 1,2,4-trichlorobenzene) as a function of applied bias. One-dimensional (1D) average conductance histograms for **P1-NH₂**, **P2-NH₂**, and **P3-NH₂** and **P1-SMe**, **P2-SMe**, and **P3-SMe** across a wide range of applied biases (-1.9 V to $+1.9$ V) are shown in Figures S4 and S5, respectively. The stability of molecular junctions across this range of applied bias is confirmed using transient, time-dependent conductance measurements using the holding mode of STM-BJ, as described below. Peak conductance values for **Pn-NH₂** and **Pn-SMe** are plotted on a semilog scale against the applied bias in Figure 1b and Figure S6. Overall, molecular conductance plots for **Pn-NH₂** and **Pn-SMe** are symmetric with respect to applied bias in the nonpolar solvent 1,2,4-trichlorobenzene.³¹

Remarkably, our results show that **P3-NH₂** and **P3-SMe** exhibit an abrupt jump in conductance at applied biases of 1 and 1.75 V, respectively (Figure 1b). In general, all molecular junctions based on **Pn-NH₂** and **Pn-SMe** show high conductance values above $10^{-2} G_0$ under high applied biases

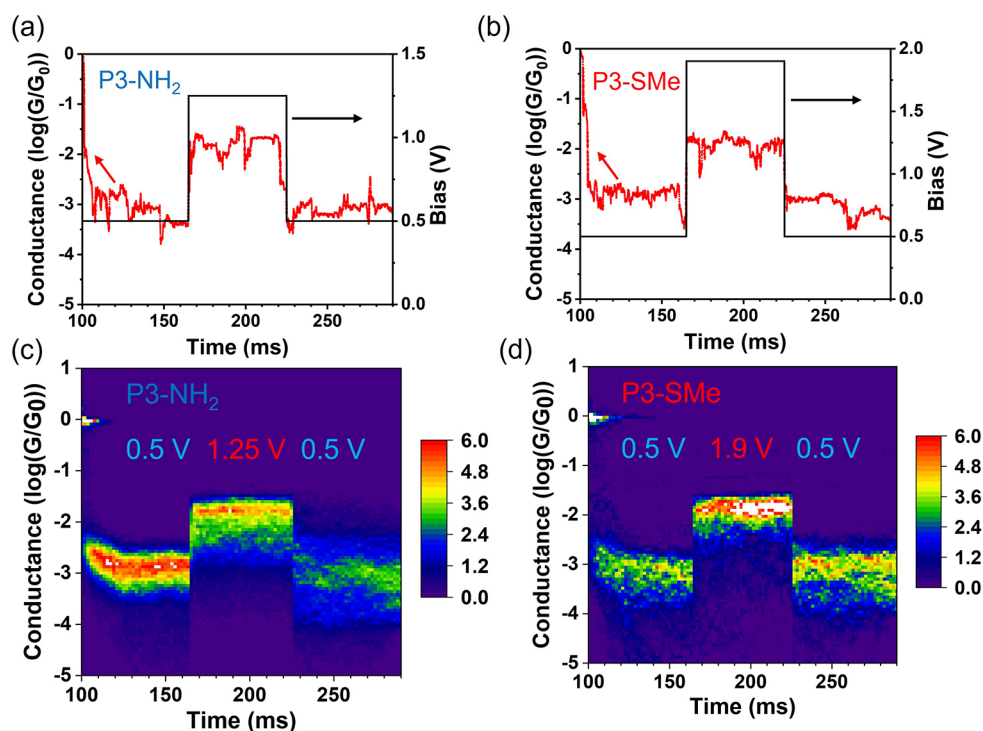


Figure 2. Transient, time-dependent bias switching experiments on single amine- and thiomethyl-terminated terphenyl junctions. (a, b) Time-dependent applied bias (black) is plotted together with characteristic transient single molecule conductance traces (red) for P3-NH₂ and P3-SMe. (c, d) 2D conductance histograms compiled from >10000 experimentally measured transient conductance traces for P3-NH₂ and P3-SMe.

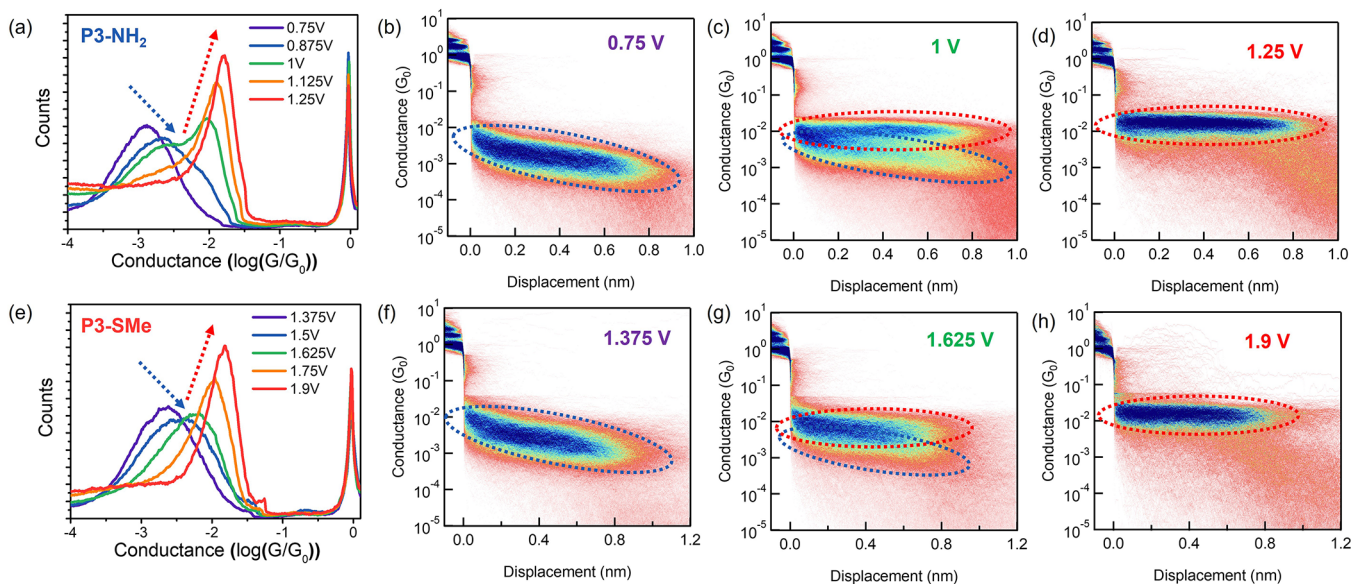


Figure 3. One-dimensional (1D) and two-dimensional (2D) conductance histograms for (a–d) P3-NH₂ and (e–h) P3-SMe at different bias voltages, each constructed from >3000 traces. Blue and red dashed line envelopes correspond to charge transport through nonresonant and resonant transport, respectively. The transition voltage (V_T) is defined as the bias voltage at which the higher G state has larger intensity than the lower G state in 1D conductance histograms, and the overall shape of the conductance plateau shifts from a downward slope to a nearly flat horizontal shape in 2D conductance histograms.

(Figure 1b and Figure S6). Using a quantum tunneling model such that $G/G_0 = A \exp(-\beta L)$, where A is a prefactor related to contact conductance, β is the molecular decay constant, and L is the molecular length between terminal carbon atoms in the junction, we determined molecular decay constants β for Pn-NH₂ and Pn-SMe as a function of applied bias. Our results show that the molecular decay constants are $\beta = 0.41 \pm 0.01$

\AA^{-1} (Pn-NH₂) and $\beta = 0.39 \pm 0.03 \text{\AA}^{-1}$ (Pn-SMe) at 0.25 V for oligophenyls, which is consistent with acetylene-terminated⁶ ($\beta = 0.38 \pm 0.03 \text{\AA}^{-1}$) and trimethyltin-terminated⁷ ($\beta = 0.43 \text{\AA}^{-1}$) oligophenyls. Surprisingly, we observe an abrupt decrease in β for P3-NH₂ at 1 V and P3-SMe at 1.75 V (Figure 1c). Decay constants decrease with increasing applied bias and become nearly length-independent at 1.9 V, such that $\beta = 0.03$

$\pm 0.03 \text{ \AA}^{-1}$ for **Pn-NH₂** and $0.07 \pm 0.01 \text{ \AA}^{-1}$ for **Pn-SMe** (Figure 1d). Moreover, the nearly length-independent molecular decay constants β at high bias are consistent with a resonant tunneling mechanism for charge transport.

Two-dimensional (2D) conductance histograms show that average molecular displacements at junction breakage increase with molecular length. In particular, 2D conductance histograms for **Pn-NH₂** and **Pn-SMe** at low bias (0.25 V) and high bias (1.9 V) are shown in Figures S7 and S8. Interestingly, **Pn-SMe** molecules generally show larger displacements compared to **Pn-NH₂** counterparts, which is consistent with prior work and is attributed to a weaker force constant between Au and SMe anchors.³² Our results further show that **Pn-SMe** exhibits a slightly larger conductance than **Pn-NH₂** at 0.25 V (Figure 1d), which agrees with prior work and is attributed to stronger coupling between SMe-terminated molecules and Au d-orbitals.³² Unexpectedly, we observe that the conductance order is reversed at high bias, such that **Pn-NH₂** molecules show significantly larger conductance values than **Pn-SMe** molecules above 1 V (Figure 1b and Figure S6), which is especially apparent for biphenyl or *p*-terphenyl junctions.

Electrochemical reactions in molecular junctions have been shown to result in conductance enhancements at high applied bias. In prior work, Zang et al. reported the formation of Au–N covalent bonds for **P3-NH₂** due to electrochemical reactions at high bias, which leads to a high conductance state.²⁰ To exclude the possibility of electrochemical-induced reactions at high applied bias, we performed time-dependent, transient measurements of molecular conductance using the holding mode of operation of the STM-BJ instrument. Here, a single molecule junction is held at a constant displacement while changing the applied bias and directly measuring conductance (Figure 2). The experiment is performed by holding a single molecule under low applied bias (0.5 V) for the initial phase (65 ms), followed by a step increase in the applied bias (1.25 V for **P3-NH₂** and 1.9 V for **P3-SMe**) for 60 ms, after which the bias is returned to the initial level (0.5 V). Figures 2c–d clearly show that the molecular conductance is reversible under controlled bias ramps. In particular, molecular conductance returns to similar levels as the initial low bias after the step change in applied bias. Overall, these results indicate that the transition or jump in molecular conductance is reversible, which strongly suggests that the molecular structures do not undergo electrochemical reactions under high applied bias.

To understand the transition bias from nonresonant to resonant transport, we performed a series of single molecule conductance experiments by increasing the bias voltage in small steps in the vicinity of the conductance jump (Figure 3). In the vicinity of the conductance jump for both **P3-NH₂** (Figure 3c) and **P3-SMe** (Figure 3g), 1D and 2D conductance histograms clearly show two underlying molecular subpopulations with different conductance values. However, at low bias, the 2D conductance plots only show the low-conductance subpopulation (Figure 3b,f), whereas at high bias, the 2D conductance plots show only the high conductance subpopulation (Figure 3d,h). Upon increasing the applied bias from 0.75 to 1.25 V, the overall shape of the conductance plateau for **P3-NH₂** in 2D conductance histograms shifts from a downward slope to a nearly flat horizontal shape (Figure 3b–d). We attribute this phenomenon to the shift from length-dependent nonresonant tunneling to nearly length-independent resonant transport. Our results suggest that two distinct conductance states exist for **P3-NH₂** and **P3-SMe**, and the

charge transport mechanism changes from nonresonant tunneling to resonant tunneling at transition voltages (V_T) corresponding to ~ 1 V for **P3-NH₂** and ~ 1.625 V for **P3-SMe**, respectively. Here, we emphasize that the transition voltage (V_T) for resonant transport is different than the transition voltage (V_{trans}) in transition voltage spectroscopy (TVS) which measures the transition from a trapezoidal barrier at low bias (Simmons tunneling) to a triangular barrier at high bias (Fowler-Nordheim tunneling).^{33,34} Typically, V_{trans} is determined as the inflection point on a plot of $\ln(G/V)$ versus $1/V$. The calculated V_{trans} for **P3-SMe** is less than 1 V, which is lower than V_T for resonant transport (Figure S9).

Prior work has shown that high bias can affect molecular conformations.^{35,36} In general, molecules with planar conformations exhibit larger average conductance values compared to their nonplanar or twisted counterparts.^{5,37} To investigate whether a bias-induced conformational change leads to a conductance jump, we synthesized a control molecule (**P3-planar**) with a “locked” and fully planar backbone conformation and determined conductance as a function of applied bias (Figure S10a). Interestingly, our results show that the conductance-voltage plot of **P3-planar** follows the same trends as **P3-SMe** (Figure S10b), and **P3-planar** exhibits a transition voltage V_T around 1.625 V (Figure S10c). At low bias (0.25 V), **P3-planar** shows a higher conductance than **P3-NH₂** and **P3-SMe** due to the planar conformation. However, at high applied bias immediately following the conductance jump for **P3-NH₂** (~ 1 V), the conductance of **P3-NH₂** is significantly larger than **P3-planar**, which indicates that the conductance jump does not result from molecular conformational changes, and the fully planar molecule (**P3-planar**) undergoes a nonresonant to resonant transition in transport.

To further understand the voltage-dependent conductance response of **P3-NH₂** and **P3-SMe**, we performed molecular modeling using nonequilibrium Green's function-density functional theory (NEGF-DFT) via the Atomistix Toolkit package. Molecular geometries for **P3-NH₂** and **P3-SMe** are optimized using DFT calculations performed on Spartan'16 Parallel Suite using the B3LYP functional with a 6-31G (d,p) basis set. Following determination of geometry-optimized structures, transmission functions and conductance-voltage ($G-V$) plots are calculated using NEGF-DFT (Figure S11). Our results show that the HOMO energy level of **P3-NH₂** is closer to the Fermi energy level E_F compared to **P3-SMe** (Figure S11b), and conductance jumps from simulations occur at ~ 1.25 V for **P3-NH₂** and ~ 1.5 V for **P3-SMe**, respectively (Figure S11c). The conductance of **P3-NH₂** increases by a factor of ~ 30 when the voltage changes from 0.5 V (nonresonant transport) to 1.5 V (resonant transport). The enhancement ratio in molecular conductance for **P3-NH₂** is consistent with experimental results (Figure 1b). Overall, the calculated $G-V$ curves are in qualitative agreement with the experimental results, although the positions and magnitudes of the conductance jumps are only qualitatively consistent with experimental values due to the asymmetry of electrodes³⁸ and the level of DFT theoretical framework.³⁹

On the basis of these observations, we sought to develop a general quantitative description for the nonresonant to resonant transition voltage V_T as a function of molecular properties. The transition voltage for resonant transport is thought to primarily depend on the alignment between the dominant frontier orbital energy and the gold electrode Fermi energy. To systematically understand the relationship between

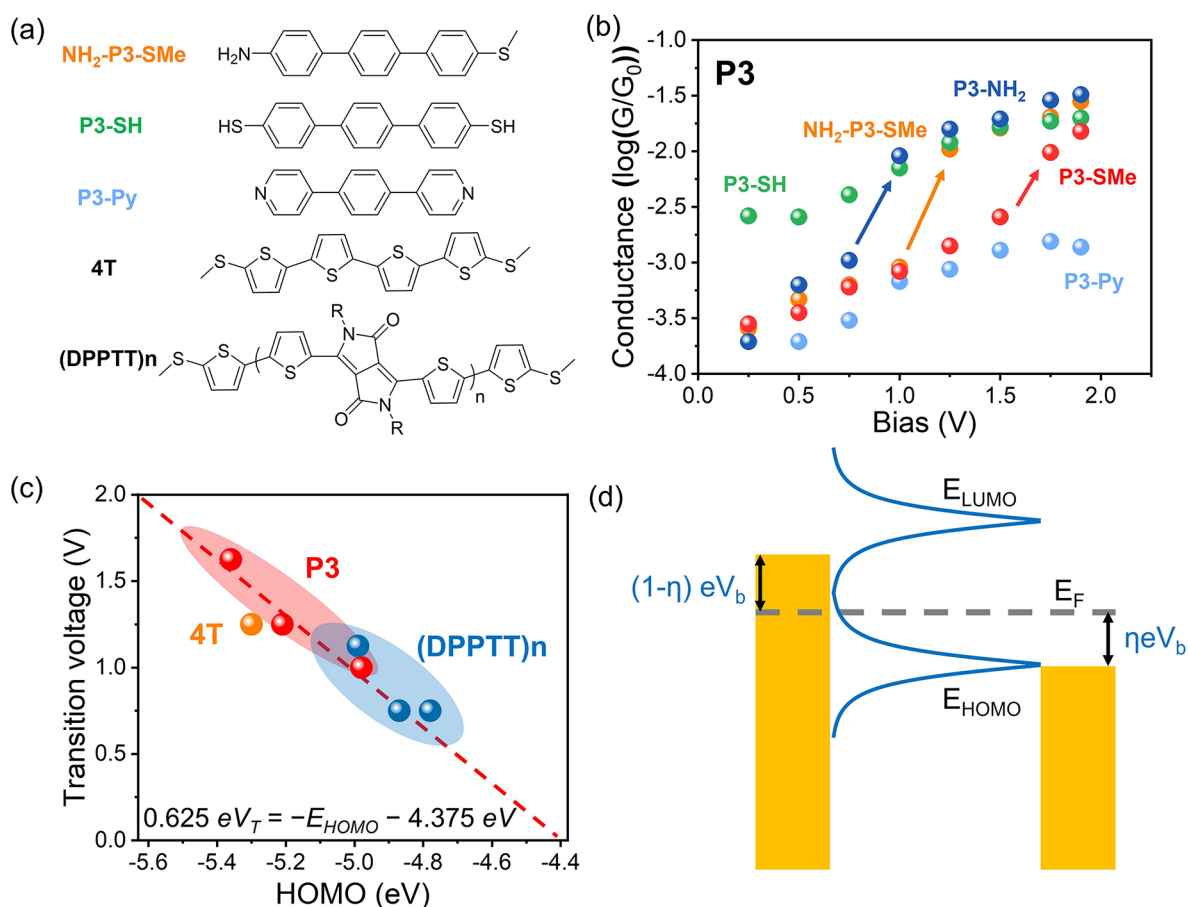


Figure 4. Understanding the relationship between transition voltage V_T and frontier molecular orbitals. (a) Series of molecules and molecular structures used in these experiments. (b) Average peak conductance values for P3 with different anchors plotted as a function of applied bias from 0.25 to 1.9 V on a semilog scale. (c) Transition voltage plotted as a function of HOMO energy levels for a series of conjugated organic molecules. (d) Schematic of energy level diagram showing alignment between the electrode Fermi energy and the HOMO energy level.

the transition voltage and frontier orbitals, we experimentally characterized molecular conductance for a series of junctions with different molecular compositions and correspondingly different HOMO and LUMO frontier energy levels (Figure 4). Specifically, we determined the conductance of 4''-(methylthio)-[1,1':4',1''-terphenyl]-4-amine (NH₂-P3-SMe), *p*-terphenyl-4,4''-dithiol (P3-SH), 1,4-di(pyridin-4-yl)benzene (P3-Py), and 4,4''-diethynyl-1,1':4',1''-terphenyl (P3-Ace) as a function of applied bias (Figure 4a and Figures S12–S13). Our results show that the conductance values of P3-SH, P3-Py, and P3-Ace smoothly and gradually increase upon increasing the applied bias without abrupt jumps, as shown in Figure 4b and Figure S13. In general, the choice of anchors affects the electronic coupling at the electrode-molecule interface. Strong electronic coupling will induce broadening of the HOMO and LUMO levels, which leads to a smooth and continuous transition from nonresonant to resonant transport.⁴⁰ Transmission functions for P3-SH, P3-Ace, and P3-Py were calculated using NEGF-DFT (Figure S14). Interestingly, we observe broad resonance states for P3-SH, P3-Ace, and P3-Py located close to the Fermi level (within ± 0.5 eV). Strong electronic coupling between electrodes and anchors (thiol, acetylene, and pyridine) generally explains the absence of an abrupt conductance jump for these molecules. P3-NH₂, NH₂-P3-SMe, and P3-SMe show abrupt jumps in molecular conductance at specific applied biases (Figure 4b). Unexpectedly, the conductance of P3-NH₂ and NH₂-P3-SMe is larger

than P3-SH at high applied bias (>1 V) after both molecules exhibit an abrupt jump in conductance (Figure 4b). In addition, the transition voltages V_T for nonresonant to resonant transport are vastly different for P3-NH₂, NH₂-P3-SMe, and P3-SMe, which suggests that V_T depends on molecular composition.

To further understand the molecular conductance data, we plotted the transition voltage V_T as a function of the HOMO energy levels for different molecules (Figure 4c and Table S1). Interestingly, our results show that the transition voltage V_T decreases with increasing HOMO energy levels (E_{HOMO}), following a linear relationship given by

$$0.625eV_T = -E_{HOMO} - 4.375eV \quad (1)$$

where e is the charge on an electron. To assess the generality of the linear relationship between V_T and E_{HOMO} given by eq 1, we further characterized the conductance and transition voltages for 4T and (DPPTT)_n with different backbone compositions, lengths, and HOMO energy levels (Figure 4a,c, Table S1, and Figures S15–S17). Interestingly, the transition voltages of these molecules are well described by the general relation, which supports the notion that the linear relationship between V_T and E_{HOMO} can be used to describe resonant transport in conjugated organic molecules.

To understand the physics governing the relationship between the transition voltage and the frontier energy levels, we consider a simple model for a molecular junction with two

gold electrodes (Figure 4d). When the Fermi energy of the gold electrodes E_F is located between the HOMO and LUMO levels, the chemical potentials of the left and right electrodes are given by $E_F - \eta eV_b$ and $E_F + (1 - \eta) eV_b$, respectively, where V_b is the bias voltage and the parameter η is related to the strength and symmetry of the molecule-electrode coupling,³⁸ such that $\eta = 0.5$ for ideal, fully symmetric junctions. To achieve resonant transport in HOMO-conducting molecules, the chemical potential of one electrode aligns with the HOMO energy level such that $E_F - \eta eV_b = E_{HOMO}$. In this way, a simple linear relationship is used to relate the HOMO energy and transition voltage such that $\eta eV_T = -E_{HOMO} + E_F$. Using this expression to analyze our experimental results, we determine the parameters $\eta = 0.625$ and $E_F = -4.375$ eV, respectively. Prior studies reported that the work function of a clean Au surface is 5.1 eV in a vacuum;⁴¹ however, the adsorption of molecules decreases the work function of gold in the range of ≈ 4.2 – 4.4 eV, as previously reported.^{42–44} In general, the calculated value of the Fermi level of gold E_F from our experiments is consistent with prior work.

The linear relationship describing the transition voltage V_T given by eq 1 is practically useful in designing molecular junctions to achieve resonant transport. In theory, our work suggests that efficient long-range transport can be achieved at low bias when the molecular HOMO energy is close to -4.375 eV. Recently, unusual length-independent conductance behaviors were reported for [*n*]cumulenes⁴⁵ and porphyrins,¹⁴ which may be related to coherent transport mechanisms in conjugated systems. In addition to conjugated molecules, Porath et al.²⁶ reported that 10.4 nm long, double-stranded DNA molecules behave like insulators at low bias and efficient conductors at high bias, such that the enhanced conductance was attributed to the alignment between the frontier molecular energy levels and E_F . However, nonconjugated molecules such as DNA typically have a large energy mismatch between the HOMO level and E_F , making it challenging to observe resonant transport given the bias range of our setup. Nevertheless, electrochemical gating⁴⁶ and selection of solvents³⁶ can be used to modulate the alignment of the conducting frontier orbital relative to the Fermi energy of the electrode, which presents exciting new avenues to understand and control resonant transport in molecular junctions.

In summary, we used a series of single molecule experiments to understand the transition between nonresonant and resonant transport in single molecule junctions. Overall, these results deepen our understanding of the relationship between molecular frontier orbitals and applied bias in single molecule junctions. Broadly, our work holds the potential to aid in the design of new materials and devices for molecular electronics and circuits.

■ ASSOCIATED CONTENT

SI Supporting Information

The Supporting Information is available free of charge at <https://pubs.acs.org/doi/10.1021/acs.nanolett.1c02915>.

Description of chemical synthesis of P2-SMe, P3-SMe, NH₂-P3-SMe, P3-planar, experimental details on STM-BJ (PDF)

■ AUTHOR INFORMATION

Corresponding Author

Charles M. Schroeder – Department of Materials Science and Engineering, Department of Chemical and Biomolecular Engineering, Department of Chemistry, and Beckman Institute for Advanced Science and Technology, University of Illinois at Urbana–Champaign, Urbana, Illinois 61801, United States; orcid.org/0000-0001-6023-2274; Email: cms@illinois.edu

Authors

Songsong Li – Department of Materials Science and Engineering and Beckman Institute for Advanced Science and Technology, University of Illinois at Urbana–Champaign, Urbana, Illinois 61801, United States

Hao Yu – Department of Chemical and Biomolecular Engineering, University of Illinois at Urbana–Champaign, Urbana, Illinois 61801, United States; orcid.org/0000-0002-1594-769X

Jialing Li – Department of Chemical and Biomolecular Engineering and Beckman Institute for Advanced Science and Technology, University of Illinois at Urbana–Champaign, Urbana, Illinois 61801, United States

Nicholas Angello – Department of Chemistry and Beckman Institute for Advanced Science and Technology, University of Illinois at Urbana–Champaign, Urbana, Illinois 61801, United States

Edward R. Jira – Department of Chemical and Biomolecular Engineering and Beckman Institute for Advanced Science and Technology, University of Illinois at Urbana–Champaign, Urbana, Illinois 61801, United States

Bo Li – Department of Chemical and Biomolecular Engineering, University of Illinois at Urbana–Champaign, Urbana, Illinois 61801, United States; orcid.org/0000-0001-9407-9503

Martin D. Burke – Department of Chemistry, Beckman Institute for Advanced Science and Technology, and Carle Illinois College of Medicine, University of Illinois at Urbana–Champaign, Urbana, Illinois 61801, United States

Jeffrey S. Moore – Department of Materials Science and Engineering, Department of Chemistry, and Beckman Institute for Advanced Science and Technology, University of Illinois at Urbana–Champaign, Urbana, Illinois 61801, United States; orcid.org/0000-0001-5841-6269

Complete contact information is available at: <https://pubs.acs.org/doi/10.1021/acs.nanolett.1c02915>

Author Contributions

S.L. conceived the study, carried out STM-BJ measurements, and performed theoretical calculations. H.Y., N.A., and E.R.J. synthesized and characterized the compounds. J.L. and B.L. helped with data analysis. C.M.S., J.S.M., and M.D.B. supervised the research. The manuscript was written by S.L. and C.M.S. with contributions from all other authors.

Notes

The authors declare no competing financial interest.

■ ACKNOWLEDGMENTS

The research was financially supported by the Joint Center for Energy Storage Research (JCESR), an Energy Innovation Hub funded by the U.S. Department of Energy, Office of Science, Basic Energy Sciences and by the U.S. Department of Defense

by a MURI (Multi-University Research Initiative) through the Army Research Office (ARO) through Award W911NF-16-1-0372 to C.M.S. and J.S.M. This work was also supported by the Defense Advanced Research Projects Agency under the Accelerated Molecular Discovery Program (Cooperative Agreement No. HR00111920027 dated August 1, 2019) to M.D.B. The content of the information presented in this work does not necessarily reflect the position or the policy of the government. Probe molecules were prepared using the Molecule Maker Lab at the Beckman Institute. N.A. is an NDSEG Graduate Research Fellow.

REFERENCES

- (1) Inkpen, M. S.; Liu, Z. F.; Li, H.; Campos, L. M.; Neaton, J. B.; Venkataraman, L. Non-chemisorbed gold–sulfur binding prevails in self-assembled monolayers. *Nat. Chem.* **2019**, *11*, 351.
- (2) Su, T. A.; Neupane, M.; Steigerwald, M. L.; Venkataraman, L.; Nuckolls, C. Chemical principles of single-molecule electronics. *Nat Rev Mater* **2016**, *1*, 16002.
- (3) Xin, N.; Guan, J.; Zhou, C.; Chen, X.; Gu, C.; Li, Y.; Ratner, M. A.; Nitzan, A.; Stoddart, J. F.; Guo, X. Concepts in the design and engineering of single-molecule electronic devices. *Nature Reviews Physics* **2019**, *1*, 211.
- (4) Yu, H.; Li, S.; Schwieter, K. E.; Liu, Y.; Sun, B.; Moore, J. S.; Schroeder, C. M. Charge Transport in Sequence-Defined Conjugated Oligomers. *J. Am. Chem. Soc.* **2020**, *142*, 4852.
- (5) Venkataraman, L.; Klare, J. E.; Nuckolls, C.; Hybertsen, M. S.; Steigerwald, M. L. Dependence of single-molecule junction conductance on molecular conformation. *Nature* **2006**, *442*, 904.
- (6) Li, S.; Yu, H.; Chen, X.; Gewirth, A. A.; Moore, J. S.; Schroeder, C. M. Covalent Ag–C Bonding Contacts from Unprotected Terminal Acetylenes for Molecular Junctions. *Nano Lett.* **2020**, *20*, 5490.
- (7) Hong, W.; Li, H.; Liu, S.-X.; Fu, Y.; Li, J.; Kaliginedi, V.; Decurtins, S.; Wandlowski, T. Trimethylsilyl-Terminated Oligo-(phenylene ethynylene)s: An Approach to Single-Molecule Junctions with Covalent Au–C σ -Bonds. *J. Am. Chem. Soc.* **2012**, *134*, 19425.
- (8) Capozzi, B.; Dell, E. J.; Berkelbach, T. C.; Reichman, D. R.; Venkataraman, L.; Campos, L. M. Length-Dependent Conductance of Oligothiophenes. *J. Am. Chem. Soc.* **2014**, *136*, 10486.
- (9) Meisner, J. S.; Kamenetska, M.; Krikorian, M.; Steigerwald, M. L.; Venkataraman, L.; Nuckolls, C. A Single-Molecule Potentiometer. *Nano Lett.* **2011**, *11*, 1575.
- (10) He, J.; Chen, F.; Li, J.; Sankey, O. F.; Terazono, Y.; Herrero, C.; Gust, D.; Moore, T. A.; Moore, A. L.; Lindsay, S. M. Electronic Decay Constant of Carotenoid Polyenes from Single-Molecule Measurements. *J. Am. Chem. Soc.* **2005**, *127*, 1384.
- (11) Sedghi, G.; García-Suárez, V. M.; Esdaile, L. J.; Anderson, H. L.; Lambert, C. J.; Martín, S.; Bethell, D.; Higgins, S. J.; Elliott, M.; Bennett, N.; Macdonald, J. E.; Nichols, R. J. Long-range electron tunnelling in oligo-porphyrin molecular wires. *Nat. Nanotechnol.* **2011**, *6*, 517.
- (12) Sedghi, G.; Sawada, K.; Esdaile, L. J.; Hoffmann, M.; Anderson, H. L.; Bethell, D.; Haiss, W.; Higgins, S. J.; Nichols, R. J. Single Molecule Conductance of Porphyrin Wires with Ultralow Attenuation. *J. Am. Chem. Soc.* **2008**, *130*, 8582.
- (13) Li, Z.; Park, T.-H.; Rawson, J.; Therien, M. J.; Borguet, E. Quasi-Ohmic Single Molecule Charge Transport through Highly Conjugated meso-to-meso Ethyne-Bridged Porphyrin Wires. *Nano Lett.* **2012**, *12*, 2722.
- (14) Leary, E.; Limburg, B.; Alanazy, A.; Sangtarash, S.; Grace, I.; Swada, K.; Esdaile, L. J.; Noori, M.; González, M. T.; Rubio-Bollinger, G.; Sadeghi, H.; Hodgson, A.; Agraït, N.; Higgins, S. J.; Lambert, C. J.; Anderson, H. L.; Nichols, R. J. Bias-Driven Conductance Increase with Length in Porphyrin Tapes. *J. Am. Chem. Soc.* **2018**, *140*, 12877.
- (15) Zang, Y.; Ray, S.; Fung, E. D.; Borges, A.; Garner, M. H.; Steigerwald, M. L.; Solomon, G. C.; Patil, S.; Venkataraman, L. Resonant Transport in Single Diketopyrrolopyrrole Junctions. *J. Am. Chem. Soc.* **2018**, *140*, 13167.
- (16) Li, B.; Yu, H.; Montoto, E. C.; Liu, Y.; Li, S.; Schwieter, K.; Rodríguez-López, J.; Moore, J. S.; Schroeder, C. M. Intrachain Charge Transport through Conjugated Donor–Acceptor Oligomers. *ACS Applied Electronic Materials* **2019**, *1*, 7.
- (17) Venkataraman, L.; Klare, J. E.; Tam, I. W.; Nuckolls, C.; Hybertsen, M. S.; Steigerwald, M. L. Single-Molecule Circuits with Well-Defined Molecular Conductance. *Nano Lett.* **2006**, *6*, 458.
- (18) Olavarria-Contreras, I. J.; Perrin, M. L.; Chen, Z.; Klyatskaya, S.; Ruben, M.; van der Zant, H. S. J. C–Au Covalently Bonded Molecular Junctions Using Nonprotected Alkynyl Anchoring Groups. *J. Am. Chem. Soc.* **2016**, *138*, 8465.
- (19) Cheng, Z. L.; Skouta, R.; Vazquez, H.; Widawsky, J. R.; Schneebeli, S.; Chen, W.; Hybertsen, M. S.; Breslow, R.; Venkataraman, L. In situ formation of highly conducting covalent Au–C contacts for single-molecule junctions. *Nat. Nanotechnol.* **2011**, *6*, 353.
- (20) Zang, Y.; Pinkard, A.; Liu, Z.-F.; Neaton, J. B.; Steigerwald, M. L.; Roy, X.; Venkataraman, L. Electronically Transparent Au–N Bonds for Molecular Junctions. *J. Am. Chem. Soc.* **2017**, *139*, 14845.
- (21) Metzger, R. M. Unimolecular Electronics. *Chem. Rev.* **2015**, *115*, S056.
- (22) Reed, M. A.; Zhou, C.; Muller, C. J.; Burgin, T. P.; Tour, J. M. Conductance of a Molecular Junction. *Science* **1997**, *278*, 252.
- (23) Di Ventra, M.; Pantelides, S. T.; Lang, N. D. First-Principles Calculation of Transport Properties of a Molecular Device. *Phys. Rev. Lett.* **2000**, *84*, 979.
- (24) RATNER, M. A.; DAVIS, B.; KEMP, M.; MUJICA, V.; ROITBERG, A.; YALIRAKI, S. Molecular Wires: Charge Transport, Mechanisms, and Control. *Ann. N. Y. Acad. Sci.* **1998**, *852*, 22.
- (25) Tans, S. J.; Devoret, M. H.; Dai, H.; Thess, A.; Smalley, R. E.; Geerligs, L. J.; Dekker, C. Individual single-wall carbon nanotubes as quantum wires. *Nature* **1997**, *386*, 474.
- (26) Porath, D.; Bezryadin, A.; de Vries, S.; Dekker, C. Direct measurement of electrical transport through DNA molecules. *Nature* **2000**, *403*, 635.
- (27) Kuang, G.; Chen, S.-Z.; Wang, W.; Lin, T.; Chen, K.; Shang, X.; Liu, P. N.; Lin, N. Resonant Charge Transport in Conjugated Molecular Wires beyond 10 nm Range. *J. Am. Chem. Soc.* **2016**, *138*, 11140.
- (28) Frisenda, R.; van der Zant, H. S. J. Transition from Strong to Weak Electronic Coupling in a Single-Molecule Junction. *Phys. Rev. Lett.* **2016**, *117*, 126804.
- (29) Li, J.; Ballmer, S. G.; Gillis, E. P.; Fujii, S.; Schmidt, M. J.; Palazzolo, A. M. E.; Lehmann, J. W.; Morehouse, G. F.; Burke, M. D. Synthesis of many different types of organic small molecules using one automated process. *Science* **2015**, *347*, 1221.
- (30) Li, S.; Yu, H.; Schwieter, K.; Chen, K.; Li, B.; Liu, Y.; Moore, J. S.; Schroeder, C. M. Charge Transport and Quantum Interference Effects in Oxazole-Terminated Conjugated Oligomers. *J. Am. Chem. Soc.* **2019**, *141*, 16079.
- (31) Capozzi, B.; Xia, J.; Adak, O.; Dell, E. J.; Liu, Z.-F.; Taylor, J. C.; Neaton, J. B.; Campos, L. M.; Venkataraman, L. Single-molecule diodes with high rectification ratios through environmental control. *Nat. Nanotechnol.* **2015**, *10*, 522.
- (32) Park, Y. S.; Whalley, A. C.; Kamenetska, M.; Steigerwald, M. L.; Hybertsen, M. S.; Nuckolls, C.; Venkataraman, L. Contact Chemistry and Single-Molecule Conductance: A Comparison of Phosphines, Methyl Sulfides, and Amines. *J. Am. Chem. Soc.* **2007**, *129*, 15768.
- (33) Beebe, J. M.; Kim, B.; Gadzuk, J. W.; Daniel Frisbie, C.; Kushmerick, J. G. Transition from Direct Tunneling to Field Emission in Metal-Molecule-Metal Junctions. *Phys. Rev. Lett.* **2006**, *97*, 026801.
- (34) Ho Choi, S.; Kim, B.; Frisbie, C. D. Electrical Resistance of Long Conjugated Molecular Wires. *Science* **2008**, *320*, 1482.
- (35) Tang, Y.; Zhou, Y.; Zhou, D.; Chen, Y.; Xiao, Z.; Shi, J.; Liu, J.; Hong, W. Electric Field-Induced Assembly in Single-Stacking Terphenyl Junctions. *J. Am. Chem. Soc.* **2020**, *142*, 19101.
- (36) Zang, Y.; Fung, E. D.; Fu, T.; Ray, S.; Garner, M. H.; Borges, A.; Steigerwald, M. L.; Patil, S.; Solomon, G.; Venkataraman, L.

Voltage-Induced Single-Molecule Junction Planarization. *Nano Lett.* **2021**, *21*, 673.

(37) Dell, E. J.; Capozzi, B.; DuBay, K. H.; Berkelbach, T. C.; Moreno, J. R.; Reichman, D. R.; Venkataraman, L.; Campos, L. M. Impact of Molecular Symmetry on Single-Molecule Conductance. *J. Am. Chem. Soc.* **2013**, *135*, 11724.

(38) Jan van der Molen, S.; Liljeroth, P. Charge transport through molecular switches. *J. Phys.: Condens. Matter* **2010**, *22*, 133001.

(39) Quek, S. Y.; Venkataraman, L.; Choi, H. J.; Louie, S. G.; Hybertsen, M. S.; Neaton, J. B. Amine–Gold Linked Single-Molecule Circuits: Experiment and Theory. *Nano Lett.* **2007**, *7*, 3477.

(40) Gehring, P.; Thijssen, J. M.; van der Zant, H. S. J. Single-molecule quantum-transport phenomena in break junctions. *Nature Reviews Physics* **2019**, *1*, 381.

(41) Michaelson, H. B. The work function of the elements and its periodicity. *J. Appl. Phys.* **1977**, *48*, 4729.

(42) Huang, B.; Liu, X.; Yuan, Y.; Hong, Z.-W.; Zheng, J.-F.; Pei, L.-Q.; Shao, Y.; Li, J.-F.; Zhou, X.-S.; Chen, J.-Z.; Jin, S.; Mao, B.-W. Controlling and Observing Sharp-Valleyed Quantum Interference Effect in Single Molecular Junctions. *J. Am. Chem. Soc.* **2018**, *140*, 17685.

(43) Kim, B.; Choi, S. H.; Zhu, X. Y.; Frisbie, C. D. Molecular Tunnel Junctions Based on π -Conjugated Oligoacene Thiols and Dithiols between Ag, Au, and Pt Contacts: Effect of Surface Linking Group and Metal Work Function. *J. Am. Chem. Soc.* **2011**, *133*, 19864.

(44) Yuan, L.; Franco, C.; Crivillers, N.; Mas-Torrent, M.; Cao, L.; Sangeeth, C. S. S.; Rovira, C.; Veciana, J.; Nijhuis, C. A. Chemical control over the energy-level alignment in a two-terminal junction. *Nat. Commun.* **2016**, *7*, 12066.

(45) Xu, W.; Leary, E.; Hou, S.; Sangtarash, S.; González, M. T.; Rubio-Bollinger, G.; Wu, Q.; Sadeghi, H.; Tejerina, L.; Christensen, K. E.; Agrait, N.; Higgins, S. J.; Lambert, C. J.; Nichols, R. J.; Anderson, H. L. Unusual Length Dependence of the Conductance in Cumulene Molecular Wires. *Angew. Chem., Int. Ed.* **2019**, *58*, 8378.

(46) Capozzi, B.; Chen, Q.; Darancet, P.; Kotiuga, M.; Buzzeo, M.; Neaton, J. B.; Nuckolls, C.; Venkataraman, L. Tunable Charge Transport in Single-Molecule Junctions via Electrolytic Gating. *Nano Lett.* **2014**, *14*, 1400.